Detection of singular wave front with a Hartmann sensor. Efficiency of an adaptive system with such a sensor

F.Yu. Kanev

Institute of Atmospheric Optics,
Siberian Branch of the Russian Academy of Sciences, Tomsk

Received October 27, 2004

In this paper I consider the effect of two key elements of an adaptive system, namely, of a Shack–Hartmann sensor and a deformable mirror, on the efficiency of correction for the atmospheric turbulence. In particular, the wave front reconstruction with such a system has been analyzed assuming no singularities in the phase of reference radiation and the phase with dislocations. It is shown that the appearance of singular points not always leads to losses in accuracy of phase detection and stability of adaptive control in the system including a real sensor and an ideal mirror. On the other hand, the use of a real mirror with a continuous reflecting surface under such conditions leads to the loss in beam control stability.

Methods of wave-front measurements and devices intended for such measurements are well-known; therefore, without considering their optical arrangement and operating algorithms in detail, I shall focus in this paper on the studies, whose authors attract attention to specific features that arise when a Hartmann sensor is used for detection of phase surface which has discontinuities.

One of the first papers, considering the appearance of optical vortices and proposing the phase reconstruction methods, was published by Fried and Vaughan in 1992.[1] This paper not only showed the problem, but also considered the ways of its solution. Later on, Barchers[2] showed that it is just the appearance of dislocations that leads to a decrease in the efficiency of phase detection with a Hartmann sensor. Similar results were also presented in other papers,[3–5] published virtually at the same time.

Some recent publications[6–8] have reported on the improved accuracy of methods for detection of vortical wave beams and compared the existing methods. Now we have sufficiently comprehensive information, necessary for the phase reconstruction to be performed.[9,10]

It is a characteristic feature of the above-mentioned papers that the methods described in them were used for reconstruction of the phase, determined as an arctangent of the ratio between the imaginary and real parts of the complex amplitude of the light field, that is, the phase before and after the reconstruction was determined at the nodes of the computational grid with the resolution much higher than that of an actual sensor.

In this paper, the algorithm for reconstructing phase with a singularity is directly included into the sensor model, describing a realistic device. In addition, the effect of a deformable mirror with the continuous reflecting surface on the adaptive beam control is estimated.

1. Detection of a preset phase surface by the Hartmann sensor and efficiency of the sensor in a phase conjugation system

The investigations, whose results are presented in this paper, were carried out by the methods of computer experiment. In the model optical experiment, a laser beam passes through a thin layer of a turbulent medium, simulated by a single phase screen, or through a distributed turbulent lens, filling the entire path from the laser output aperture to the observation plane. In the case of a single screen, its position on the path, i.e., the distance Z_s from the screen to the laser, varies. The intensity of atmospheric turbulence is characterized by the Fried radius

$$r_0 = \left(0.423k^2 \int_0^L C_n^2(l)\, \mathrm{d}l \right)^{-3/5},$$

where L is the thickness of the turbulent layer; C_n^2 is the structure constant of the atmosphere; k is a constant. To characterize the residual distortions and the efficiency of compensation, the following focusing criterion was used:

$$J(t) = \frac{1}{P_0} \iint \rho(x, y) I(x, y, z_0, t)\, \mathrm{d}x\mathrm{d}y,$$

which is the fraction of light power, concentrated within the aperture of the radius a_0. Here P_0 is the total beam power;

$$\rho(x, y) = \exp\left(-(x^2 + y^2)/a_0^2\right)$$

is the function of aperture.

0235-6880/04/12 904-09 $02.00

The results reported in this paper were obtained with the system model including, in its turn, two models of the Hartmann sensor, which are described in Refs. 3 and 4. The first model is simplified; it is easy to adjust and is characterized by higher accuracy. At the same time, this model is quite far from a realistic device.

The second model is much closer to an actual device, but one faces serious difficulties in using this model. In particular, the accuracy of phase reconstruction decreases significantly, if the detection plane does not coincide with the plane, onto which the lenslet array focuses beams. In addition, limitations of the dynamic range manifest themselves to a larger degree, and the model has a somewhat lower accuracy. Therefore, the following technique was used to obtain the results. All the data were calculated using the simplified and more reliable model. Then the main dependences were tested with the use of the second model.

At the initial stages, both of the sensors employed the same algorithms of sewing together the phase surfaces. Figure 1 shows schematically the process of sewing together the phase surfaces of tilts detected at subapertures.

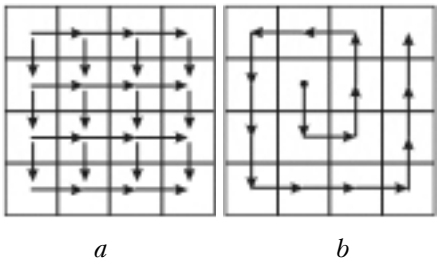

Fig. 1. Schematic presentation of the phase surface reconstruction algorithms. Strip sewing (*a*) and spiral sewing (*b*).

In the first version, strips were formed of subapertures based on the least-squares method and then those were sewed together (Fig. 1*a*). In the second version, the sewing of sensor elements together was performed along a spiral, as shown in Fig. 1*b*.

It is known that to compensate for atmospheric turbulence and thermal blooming, i.e., in the cases when a system including the sensor is to be used, it is sufficient to specify the phase by the first Zernike polynomials.[11,12] Therefore, it is worth studying the accuracy of detecting these polynomials with a sensor. The results of numerical experiments on the deviation of the obtained phase surface from the preset one as a function of the number of subapertures, are shown in Fig. 2.

The deviation was characterized by the square error ε, defined as

$$\varepsilon = \left(\sum_{i=1}^{M} \sum_{j=1}^{M} (\varphi_{i,j} - \psi_{i,j})^2 \Big/ \sum_{i=1}^{N} \sum_{j=1}^{N} \varphi_{i,j}^2 \right)^{1/2},$$

where M is the dimension of the computational grid; φ is the surface resulting from detection; ψ is the surface to be detected. The calculations were performed with the use of the second model of the sensor (prototype of an actual device), both of the methods described above were applied for sewing, but the accuracy was found independent of the sewing algorithm used.

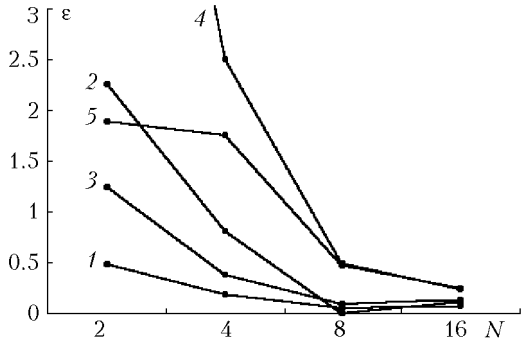

Fig. 2. Accuracy of detection of the phase surface given by the first Zernike polynomials as a function of the number of sensor subapertures; ε is the square error; N is the number of sensor subapertures along one of the coordinate axes ($N \times N$ lenslet array is used): tilt (curve *1*), defocus (*2*), astigmatism (*3*), coma (*4*), and spherical aberration (*5*).

The data presented show that at $N = 8$ (8×8 lenslet array) the accuracy of detection of the tilt, astigmatism, and focusing remains satisfactory within the error better than 10%. The worst results were obtained for coma and spherical aberration, for which ε is roughly equal to 0.5 (50%). If a 16×16 lenslet array is used, the accuracy still does not improve. The idealized model of the sensor gives 5–7% lower error, but still does not change radically the tendencies obtained.

If an increase in N leads to a decrease in the size of a lens, then the dynamic range of the sensor indirectly depends on the number of subapertures. This is illustrated in Fig. 3, from which we can see that at $N = 16$ the tilts at the phase surface edges are detected incorrectly.

Having considered the detection of the phase surface given by the lower polynomials, let us pass on to the analysis of the possibility of using the sensor in the systems intended for correction for the atmospheric distortions. Figure 4 depicts a typical phase profile of the beam transmitted through a turbulent screen at one of the realizations. The detection of this profile by the sensor is illustrated in Fig. 5, which shows the reconstructed surface, obtained at different dimensions, and its cross section.

At 16×16 number of subapertures, we can see both visually and from the distribution over the cross section that the sensor rather accurately detects the surface, although the cross section shows the limited range and the related appearance of errors at the edges. The decrease of the dimension worsens the accuracy, and the tilt within a subaperture only approximates the actual profile. It is clearly seen for the 4×4 aperture.

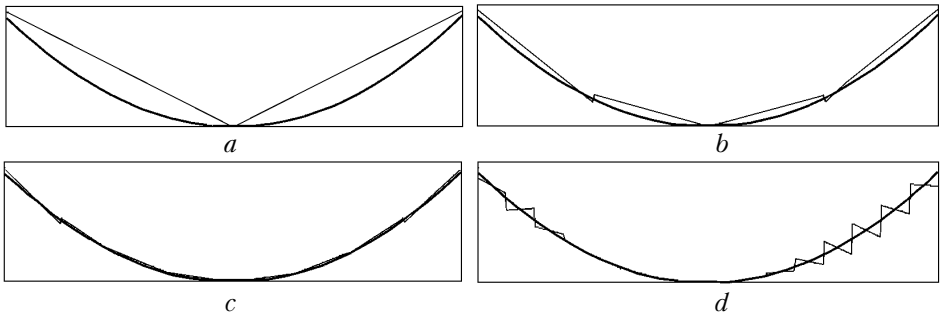

Fig. 3. Illustration of the accuracy of detection of the phase surface for defocus taken as an example: preset surface (bold line), restored surface (thin line); the number of subapertures is 2×2 (*a*), 4×4 (*b*), 8×8 (*c*), and 16×16 (*d*).

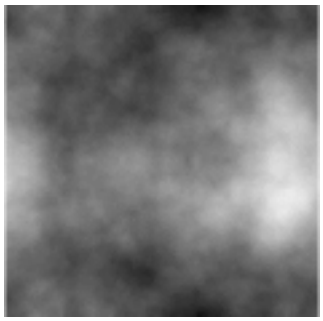

Fig. 4. Phase surface to be reconstructed.

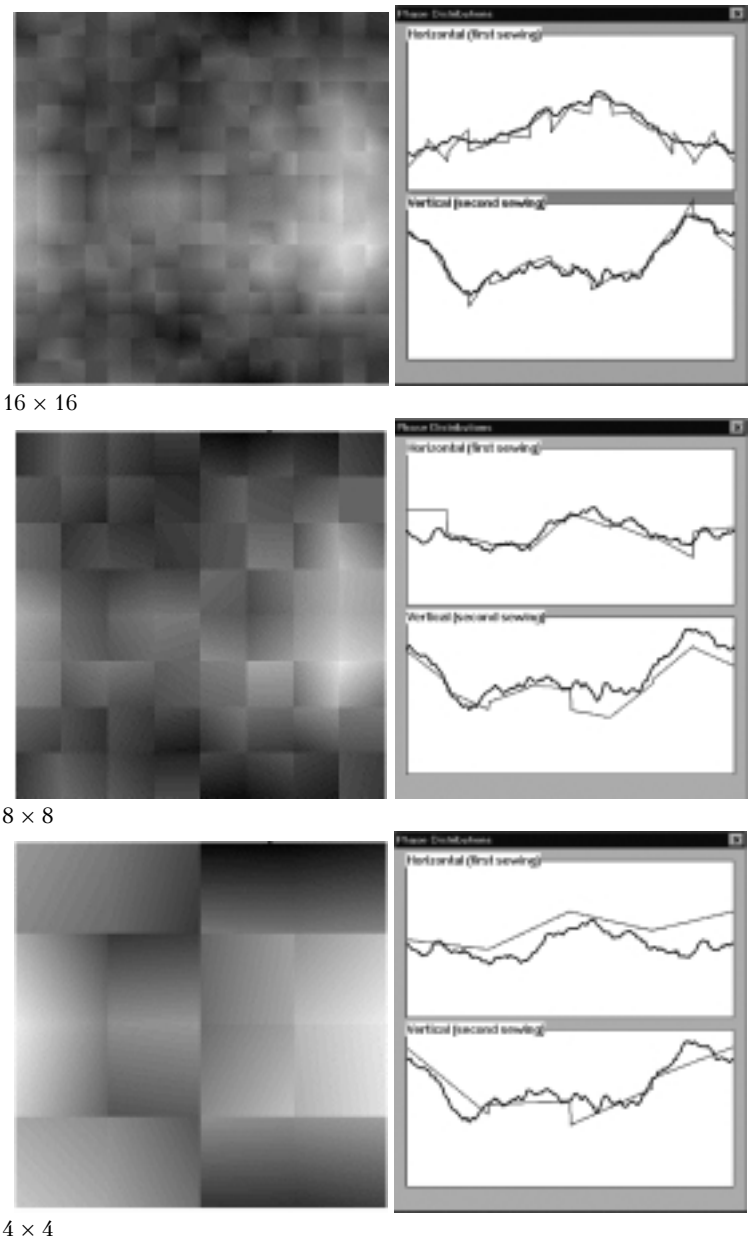

Fig. 5. Reconstruction of the phase surface by the Hartmann sensor: (left column) reconstructed surface, (right column) horizontal and vertical cross sections of the reconstructed surface (bold line) and the surface detected by the sensor (thin line). The number of sensor subapertures is given near the figures.

The errors in the phase reconstruction decrease the efficiency of compensation for the atmospheric turbulence. This is shown in Fig. 6, which depicts the dependence of the focusing criterion J, obtained from the phase conjugation in the ideal adaptive system (curve *1*) and in the system, including the Hartmann sensor with an 8×8 lenslet array (curve *2*), on the intensity of turbulent distortions. The distorting phase screen is located at the beginning of the path, which means that there are no dislocations in the wave front of the reference radiation.

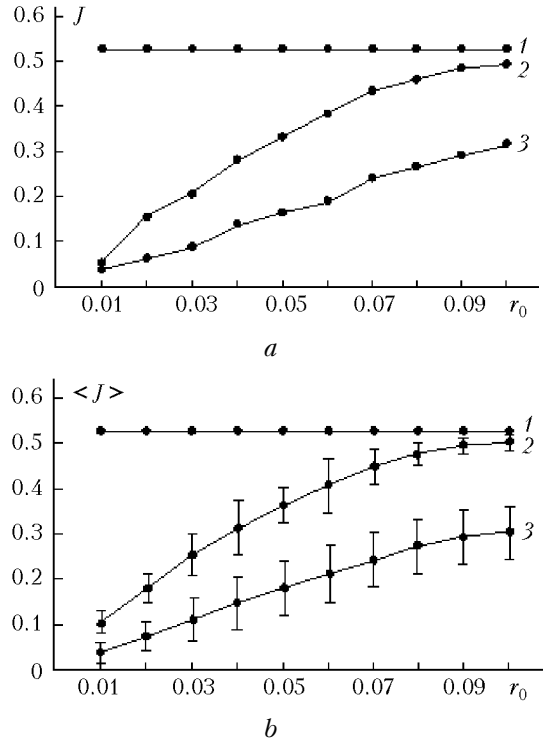

Fig. 6. Efficiency of compensation for the atmospheric turbulence as a function of the intensity of distortions for one of the realizations of the random phase screen (*a*) and after averaging over 50 realizations (*b*). Turbulence is simulated by a single screen, located at the beginning of the path; the path length is $z = 0.5$, J is the focusing criterion, r_0 is the Fried radius; ideal system (curve *1*), system including the sensor (*2*), and system without a control (*3*).

With the increase of the turbulence intensity and the complexity of the phase to be reconstructed (decrease of r_0), the efficiency of conjugation decreases markedly, and at $r_0 = 0.01$ the control of the beam allows the concentration of light field in the observation plane to be increased. At the same time, at the moderate or low distortions, the sensor provides for the focusing criterion two and more times higher than the results obtained without adaptive control (comparison of curves *2* and *3*).

The results presented suggest that, in the absence of singularities and the relevant number of subapertures, the Hartmann sensor gives quite satisfactory quality of compensation for the turbulent distortions.

2. Influence of dislocations on the accuracy of phase reconstruction with a Hartmann sensor

In Refs. 13 and 14, it was shown that dislocations arise in the phase of the beam, which has traveled a finite (greater than zero) distance behind the distorting screen. Therefore, by placing the screen in the source aperture plane, we provided for the absolute absence of singular points in the reference radiation. If the phase screen is located at the center of the propagation path and the path length amounts to a half of the diffraction length, then optical vortices arise in the wave front of the reference radiation.

The results obtained with the use of the adaptive phase-conjugation system intended for compensation of one realization of the two-dimensional field of random distortions are shown in Fig. 7*a*, while Fig. 7*b* shows the averaged data.

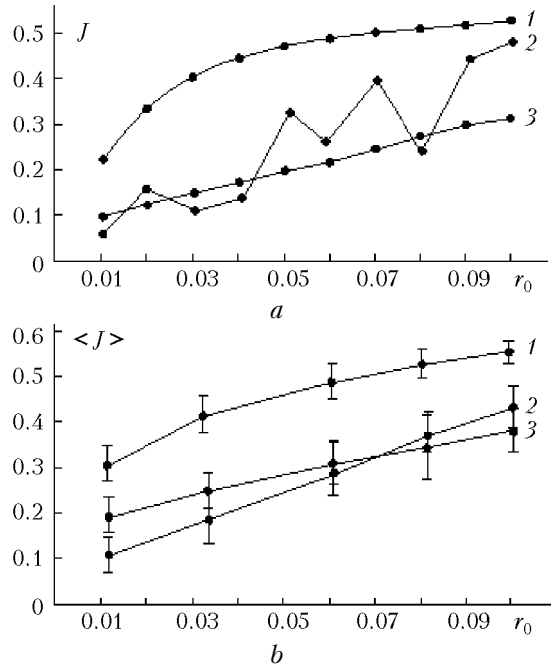

Fig. 7. Efficiency of the phase conjugation system, including a sensor, in the presence of dislocations in the phase profile of the reference radiation; the propagation path is $z = 0.5$; turbulence is simulated by a single screen located at the center of the path; data for one realization of the phase screen (*a*) and after averaging over 50 realizations (*b*); results of the control with an ideal sensor (curve *1*), the sensor with 8×8 lenslet array (*2*), and without a control (*3*).

Curve *1* corresponds to the ideal sensor, i.e., the device, in which the phase is calculated as $\arctan(\mathrm{Im}(E)/\mathrm{Re}(E))$, where $\mathrm{Im}(E)$ is the imaginary part of the complex amplitude of the light field and $\mathrm{Re}(E)$ is the real one. The accuracy of detecting the phase profile in this case is determined only by the dimension of the computational grid and it is independent of the presence of dislocations. Nevertheless, the resulting values of the focusing criterion are lower than at the complete compensation

for the distortions, when J was equal to 0.53. This can be explained by violation of the optical reciprocity principle at the phase conjugation.

The results obtained with the use of the sensor in the adaptive phase-conjugation system are shown by curve *2* in Fig. 7. We can see that the control in this case is unstable and the variation of the intensity of turbulent distortions leads to oscillations of the focusing criterion at individual realizations (Fig. 7*a*, curve *2*) and to a decrease of the average values (curve *2* in Fig. 7*b*). The decrease of the average values of the criterion can be so significant that higher concentration of the light field in the observation plane can be achieved with the feedback loop turned off. Let us explain the obtained plots.

In the phase-conjugation system, including a sensor compensating for the distortions introduced by the screen placed at the center of the propagation path, there are three sources of errors:

1. Violation of the optical reciprocity principle, leading to incomplete compensation for the aberrations.
2. Limited resolution of the sensor and the related errors in detection of a smooth (without discontinuities) phase profile.
3. Errors caused by the presence of dislocations.

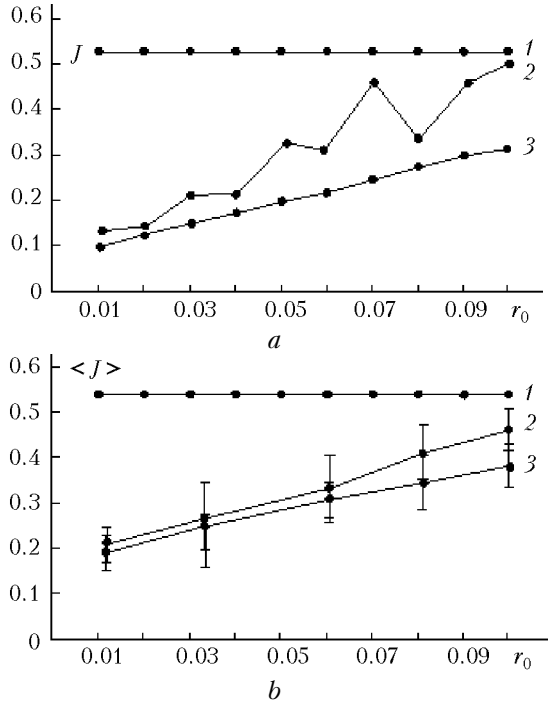

Fig. 8. Sensor included into the amplitude-phase control system; parameters are the same as in Fig. 7; results of the control with the ideal sensor (curve *1*), the sensor with 8×8 lenslet array (*2*), and without a control (*3*).

The errors of the first type can easily be excluded. To do this, an optical layout is needed, in which the beam amplitude at the medium entrance is set equal to the amplitude of the reference signal, and the phase profile of a beacon is detected with the sensor. Note that this experiment corresponds to the sensor included into a two-mirror adaptive system.[15] The results of correction for distortions in this model are shown in Fig. 8. Here the ideal sensor provides for the absolute compensation for the phase screen (curves *1* in Fig. 8), whereas an actual device again leads to oscillations of the criterion in individual realizations (curve *2*, Fig. 8*a*) and to the decrease of the average values (curve *2*, Fig. 8*b*). Thus, the fulfillment of the optical reciprocity principle does not guarantee a radical increase of the criterion.

The errors of the second type also cannot lead to the loss of stability in the phase control. In the previous section it was shown that the limited sensor resolution leads to a poorer field concentration, and the criterion decreases monotonically with the increase of the intensity of the distortions. No oscillations and losses of control stability were observed in this case.

The third source of errors is the presence of singular points in the wave front. The ideal sensor does not react to them, while in an actual device those cause a decrease of its efficiency.

3. Principal possibility of detecting a phase surface with discontinuities

To understand why the adaptive system, including the sensor, looses the efficiency in the presence of dislocations in the wave front, we used a phase profile, having an artificial singular point, as a screen, introducing the distortions. The distorting screen is shown in Fig. 9*a*, while Fig. 10*a* depicts the amplitude distribution of the Gaussian beam, propagated through the path with this screen placed at its beginning.

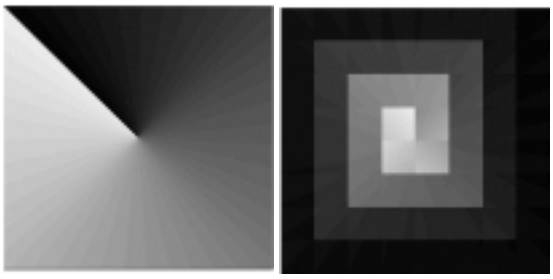

Fig. 9. Illustration of the sensor operation with the use of the spiral sewing algorithm: detected (*a*) and reconstructed (*b*) phase surfaces.

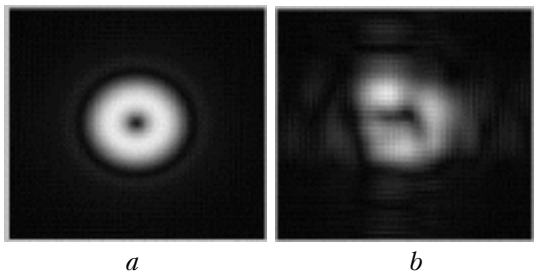

Fig. 10. Correction of the phase screen, including an artificial dislocation; light field distribution in the observation plane, obtained for the beam passed through the screen (*a*) and after correction for the screen (*b*); the sensor operates based on the spiral sewing algorithm; the path length is $z = 0.5$.

Distortions were compensated for based on the phase-conjugation algorithm. The system included the sensor, in which the sewing of the subapertures together was performed along a spiral (the direction of sewing is shown in Fig. 1*b*). The surface, obtained by wave front reconstruction with the sensor, had no singularities (Fig. 9*b*), i.e., differed significantly from the detected profile. Naturally, the adaptive control of the beam did not lead to compensation for the distortions (Fig. 10*b*). The application of the second reconstruction algorithm (see strip sewing in Fig. 1*b*) also yielded negative results.

Although we failed to compensate for the distortions, we assumed that the Hartmann sensor detects local tilts quite accurately, and the reconstruction errors are caused by the sewing together algorithm, which matches the segment sides located at the edges of phase surface discontinuity. To prove this assumption, the phase reconstruction algorithm was changed. In the modified method, a dislocation point was determined, and then a straight line, corresponding to the discontinuity, was drawn from this point in an arbitrary direction. Subapertures, separated by this line, were not sewed together. The scheme of this algorithm is shown in Fig. 11*a*, and the reconstructed surface is depicted in Fig. 11*b*.

We can see that because the direction is chosen arbitrarily, the discontinuity is shifted, but in the other relations, the preset and the resulting surfaces are identical. The sensor operating based on this algorithm, when included into the system, provided for high quality of compensation for the distortions, introduced by the screen having one singular point.

The algorithm proposed can also be used in the case of more than one singular points. In this case, it is necessary to determine the orientation of each optical vortex and to draw the discontinuities between points, having the opposite orientation. Otherwise, the technique remains the same.

Fig. 11. Algorithm of sewing together the surfaces, having a discontinuity: scheme of the algorithm (*a*), surface (*b*), and the result of sewing (*c*).

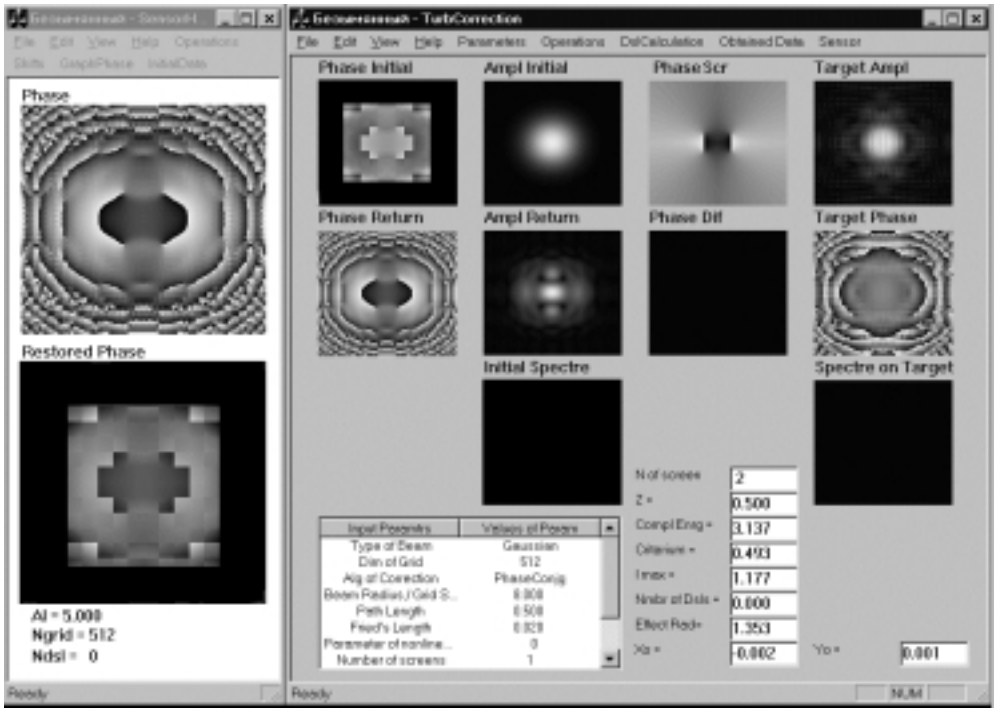

Fig. 12. Interface of the program, simulating the system with the sensor; Phase Return window demonstrates the phase profile of the reference radiation; Phase Initial window displays the surface reconstructed using the sensor; Phase Scr window shows the distorting phase screen.

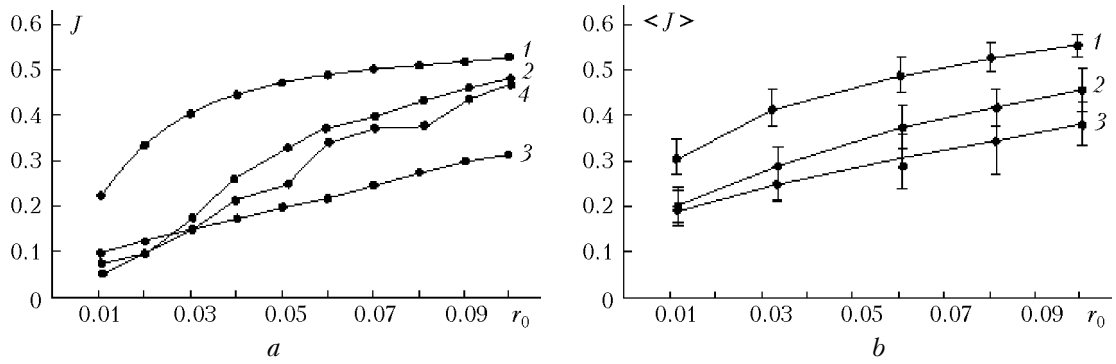

Fig. 13. Efficiency of the phase conjugation system including the sensor in the presence of dislocations in the phase profile of the reference radiation; the propagation path $z = 0.5$; turbulence is simulated by one screen located at the center of the path: (*a*) data obtained for one of the realizations of the phase screen, (*b*) data averaged over 50 realizations; result of control with the ideal sensor (curve *1*); with the sensor having a 16×16 lenslet array (*2*), and with the sensor having an 8×8 lenslet array (*4*), and without a control (*3*).

The result of surface reconstruction by use of the sensor and the correction for distortions introduced by the screen with four singular points are illustrated in Fig. 12, which shows the interfaces of the programs simulating the beam propagation through a distorting medium and the Hartmann sensor (left panel).

The distorting phase screen is displayed in the Phase Scr window, while the Target Ampl window shows the intensity distribution of the laser beam in the observation plane, obtained after the correction. The path length is 0.5; the screen is placed at the path center.

The amplitude distribution of the beam corresponds to the time, when the adaptive correction is already completed. The idea of the distortions can be gained from the amplitude distribution of the reference beam, shown in the Ampl Return window. In this case, the control has provided for high accuracy of compensation for the aberrations, and the resulting beam (Target Ampl window) is almost Gaussian. Certainly, the correction is not absolute, because the distorting layer is located at the path center and to compensate for it, the amplitude-phase beam control methods should be used.

The results of adaptive beam control in the system, including a sensor operating based on the modified sewing algorithm for the phase surface, are shown in Fig. 13. This figure is analogous to Fig. 7, which also shows the focusing criterion obtained upon the correction for the turbulent screen located at the center of the control path, but this scenario of the computer experiment differs by the presence of singular points in the reference radiation.

Comparing Figs. 13 and 7, we can note that the modification of the algorithm resulted in a decrease of the criterion oscillations in an individual realization upon the variation of the intensity of turbulent distortions, as well as in higher average values, which now exceed the values observed with feedback loop off (without a control).

Summarizing this section, it should be noted that the proposed algorithm, enabling one to reconstruct discontinuous phase surfaces, is not universal, and it will likely lead to errors, if the discontinuities introduced are far from real ones.

4. Complete model of the system. Efficiency of the adaptive beam control

The introduction of a deformable mirror into the model gave the expected results. In particular, the use of the corrector with a small number of actuators gave rise to additional errors in the phase reconstruction using the sensor–mirror system.

This is illustrated in Fig. 14, which shows the rms deviation ε, obtained in detecting the phase profile, specified by the first Zernike polynomials (tilt, defocus, astigmatism, coma, spherical aberration).

In the numerical experiments, whose results are shown in Fig. 14, the number of the subapertures and actuators was changed. It can be seen that for the 2×2 lenslet array the error is mostly determined by the sensor, while the addition of the mirror can lead to only slight (3–4%) increase of ε. With the increase of the accuracy of wave front detection due to the increase in the number of subapertures, the effect of the corrector becomes more pronounced.

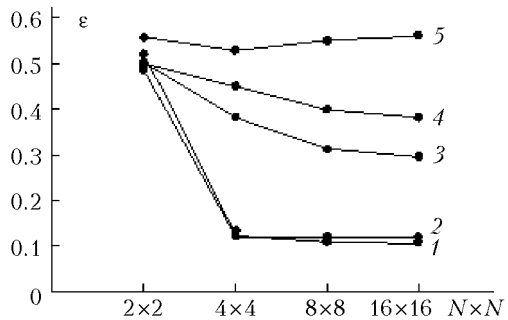

Fig. 14. Accuracy of detection of the phase profile by use of the sensor and reconstruction by the mirror: accuracy of detection (errors introduced by the mirror are neglected) (curve *1*); accuracy of reconstruction of the detected phase by the sensor–mirror system, including a corrector with 49 actuators (*2*), 21 actuators (*3*), 9 actuators (*4*), and 5 actuators (*5*).

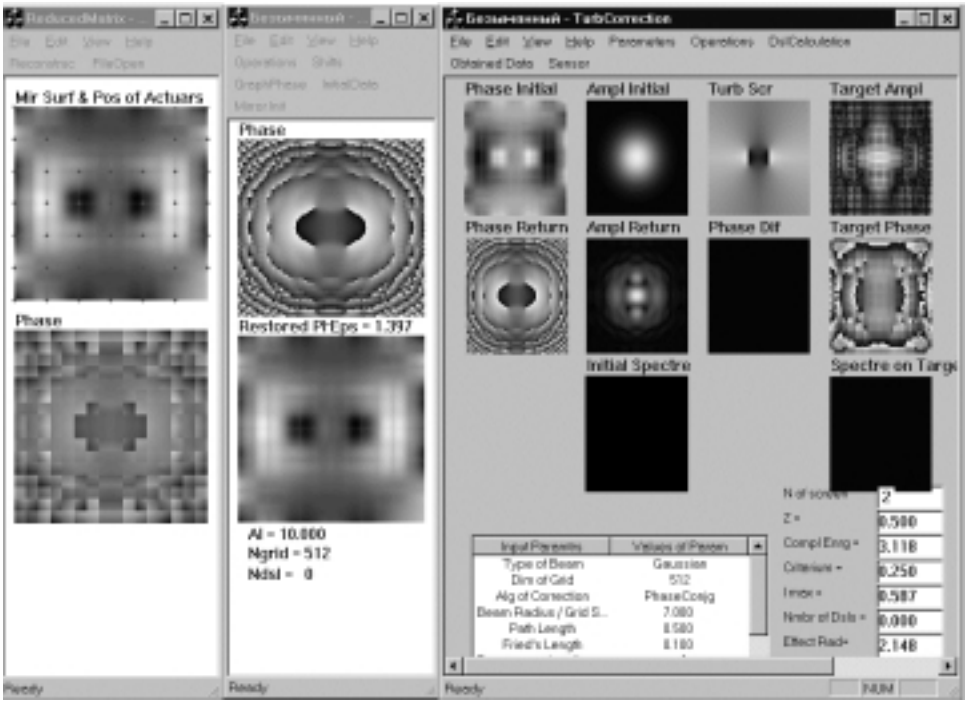

Fig. 15. Correction for the phase screen with artificial dislocations by use of the complete model of an adaptive system. Program interfaces from the right to the left: model of mirror, model of sensor, and model of beam propagation through a distorting medium.

Thus, for the 4×4 and larger lenslet array, the mirror with 5 actuators gives practically the same values of ε, varying from 50 to 60%. Despite the error of the sensor itself in no larger than 10% in this region, the accuracy of the complete system is very low and restricted just by the mirror.

The rms error introduced by the corrector can be decreased due to the increase in the number of its degrees of freedom. This is illustrated in Fig. 14, which also shows the values of ε for the sensor–corrector system, including the corrector with 9 and 21 actuators (curves *4* and *3*). The further increase in the number of degrees of freedom allows the error introduced by the mirror to be decreased almost down to zero (curve *2*).

The situation changes, if dislocations arise in the beam. Consider how the system operates under these conditions. The first stage of the investigations was carried out based on the model problem, as described above. The phase screen having singular points was set at the propagation path; the control was carried out based on the phase conjugation algorithm. It was shown above that the sensor allows these distortions to be compensated for. However, the addition of the mirror with 49 actuators has led to the loss in the efficiency of this algorithm.

Figure 15 shows the interface of the program, simulating the complete adaptive system.

The result of correction is the field distribution displayed in the Target Ampl window. Comparing it with the corresponding window of the interface shown in Fig. 12, we can see that, unlike the previous case, the beam is not focused in the system under consideration. The reason is likely the new element added to the system, namely, the adaptive mirror.

The efficiency of compensation for the turbulent screen with the use of the complete model is illustrated in Fig. 16.

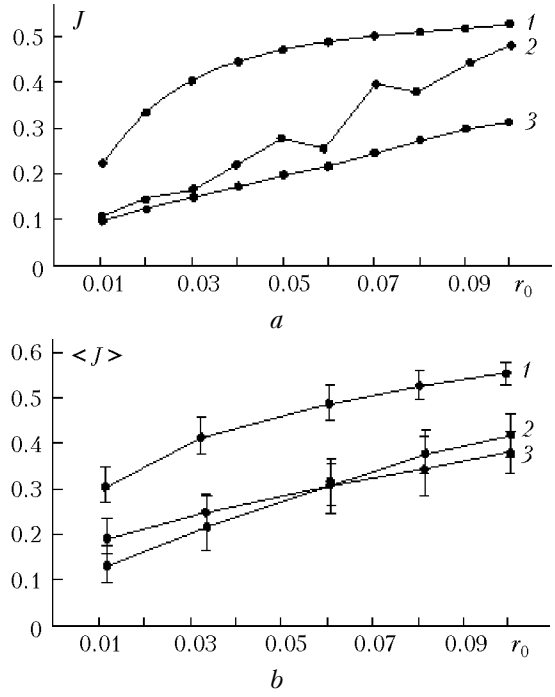

Fig. 16. Efficiency of the phase conjugation system, including the Hartmann sensor, which operates based on the modified algorithm of sewing together, and the deformable mirror: the data for one of the realizations (*a*) and the averaged results (*b*).

The distorting screen was placed at the center of the path, and the reference beam included singular points. We can see that the dependence of the focusing criterion on the intensity of turbulent distortions is nonmonotonic in an individual realization (curve *2* in Fig. 16*a*). Recall that for the ideal sensor we have obtained the dependence without oscillations of the criterion (see Fig. 13). In addition, the errors introduced by the mirror have led to a decrease in the average values. This can be seen from the comparison of Figs. 13*b* and 16*b*.

Conclusions

In this paper, the operation of a complete adaptive system, that is, the system including a beam propagation path, a wave front sensor, and a deformable mirror, has been considered for the first time. The results obtained suggest the following conclusions:

1. The accuracy of detection of a wave front having no singular points by a Hartmann sensor depends on the number of its subapertures. On the other hand, an increase in the dimension of the lenslet array of the sensor leads to a decrease of its dynamic range. Therefore, for the sensor there is no unique dependence of the accuracy on the dimension of the lenslet array.

2. In the presence of dislocations, the possibility of detecting the beam phase profile by the sensor is determined by the algorithm of sewing together used. This paper proposes the algorithm of sewing together capable of detecting discontinuous wave fronts.

3. The use of the modified algorithm of sewing together allows the turbulent distortions to be compensated for with the high efficiency by the system including the sensor and an ideal (specifying the phase profile without restrictions) mirror.

4. The addition of a deformable mirror with several tens (about 50) degrees of freedom to the adaptive system does not lead to a decrease in the efficiency of correction for turbulent distortions when there are no dislocations. The use of the corrector with a smaller number of actuators (20 and less) can cause a loss in the beam control efficiency.

5. If the system includes a mirror with the continuous reflecting surface and a relatively small number (about 50) of degrees of freedom, then the presence of singular points in the phase profile of the reference beam leads to a decrease in the quality of compensation for the turbulent distortions. This is caused just by the mirror, because the Hartmann sensor operated following a modified algorithm of sewing together is quite accurate under these conditions.

References

1. D.L. Fried and J.L. Vaughan, Appl. Opt. **31**, No. 15, 2865–2882 (1992).
2. J.D. Barchers, D.L. Fried, and D.J. Link, Appl. Opt. **41**, No. 6, 1012–1021 (2002).
3. F.Yu. Kanev, V.P. Lukin, and N.A. Makenova, Atmos. Oceanic Opt. **15**, No. 11, 926–933 (2002).
4. F.Yu. Kanev, V.P. Lukin, and N.A. Makenova, Proc. SPIE **5026**, 190–197 (2002).
5. F.Yu. Kanev, V.P. Lukin, and N.A. Makenova, in: *Proc. of Intern. Conf. on Remote Sensing* (Greece, 2002), p. 52.
6. M.C. Roggemann and A.C. Koivunen, J. Opt. Soc. Am. A **17**, No. 5, 911–919 (2000).
7. M.C. Roggemann and A.C. Koivunen, J. Opt. Soc. Am. A **17**, No. 1, 53–62 (2000).
8. G.C. Dente, Appl. Opt. **39**, No. 10, 1480–1484 (1999).
9. D.L. Fried, *"Complex exponential reconstructor with RMS-noise weighted error-reduction: A solution to the branch point reconstruction problem,"* Report No. TN-092 (1999).
10. D.L. Fried, *"Using the hidden phase formulation in wave front reconstruction,"* Report No. TN-100 (1999).
11. R.J. Noll, J. Opt. Soc. Am. **66**, No. 3, 207–211 (1976).
12. F.Yu. Kanev and S.S. Chesnokov, Atm. Opt. **4**, No. 9, 689–691 (1991).
13. F.Yu. Kanev, V.P. Lukin, and N.A. Makenova, Proc. SPIE **4357**, 231–235 (2001).
14. F.Yu. Kanev, V.P. Lukin, and L.N. Lavrinova, Proc. SPIE **4357**, 244–249 (2001).
15. F.Yu. Kanev, V.P. Lukin, and N.A. Makenova, Atmos. Oceanic Opt. **15**, No. 12, 973–977 (2002).